Appl. Magn. Reson. (2008) 35, 185–195
DOI 10.1007/s00723-008-0151-3
Printed in The Netherlands

Applied
Magnetic Resonance

Ultracompact NMR: ^{1}H Spectroscopy in a Subkilogram Magnet

A. McDowell and **E. Fukushima**

ABQMR Inc., Albuquerque, New Mexico, USA

Received 21 March 2008; revised 9 June 2008

Abstract. We demonstrate the first subkilogram permanent magnet and microcoil probe combination capable of ^{1}H nuclear magnetic resonance spectroscopy with subparts-per-million resolution. The 1 T magnet with a weight of 685 g utilizes steel pole faces and flux return paths to provide a sufficiently homogeneous magnetic field in a robust, easy-to-use device nearly immune to environmental influences. The microcoil probe provides a signal-to-noise ratio of 61 in a single data acquisition from 21 nanoliters of water. The line width achieved, 0.24 ppm, can be explained by the measured field variations across the sample volume. The device does not have shim coils, temperature insulation and control, or adequate radio frequency shielding, so simple improvements in these areas will lead to further increases in performance. When combined with commercially available miniaturized electronics, the magnet and the probe described here will form the first handheld device capable of ^{1}H spectroscopy.

1 Introduction

In the past sixty years, nuclear magnetic resonance (NMR) has developed into a behemoth, both in terms of its influence in science and clinical medicine as well as its size and cost. A major reason for its popularity is its broad applicability to the study of chemical, physical, and spatial properties of samples without damaging or destroying them. NMR spectroscopy, in particular, is a powerful analytical chemistry tool. The potential value of NMR in applied industrial settings has long been recognized [1–5] and the development of the techniques and hardware to enable "factory-floor" applications remains a minor but significant subspecialty of the field [6–13]. This note describes a substantial step forward in this effort: the first handheld ($<$1 kg) NMR magnet and probe capable of ^{1}H spectroscopy at a resolution of 0.24 parts per million (ppm).

Industrial applications of NMR require compact, rugged systems that are insensitive to their environment, inexpensive, and easy to use and maintain. Nearly all commercially available compact systems are based on permanent magnets. (Compact superconducting magnets are available [14] but have seen limited use.)

Most of the commercial devices (a partial list includes Bruker's minispec, Oxford's Maran Ultra, Resonance System's SpinTrack, Stellar's SMARTracer, Progression's MagModule II) are used to determine the relaxation times of samples, an approach compatible with the low-homogeneity fields typical of small permanent magnets. These relaxation times, or their distributions, can be correlated with parameters of interest in industry. However, these systems would be even more useful if they could perform ^{1}H spectroscopy, which requires a minimum of 1 ppm resolution. At least one device capable of spectral resolution is available [15], albeit in form factor too large (about 1000 kg) to be portable. The power of NMR as a spectroscopic tool in the industrial setting remains largely unrealized due, in large part, to the inherently low sensitivity of the NMR signal generation process and the difficulties of making small permanent magnets with sufficiently homogeneous magnetic fields.

In order to overcome these difficulties, we have combined recent advances in microcoil NMR detectors and permanent magnet technologies. Microcoil NMR for volume-limited samples in high-field superconducting magnets has existed for about 15 years [16]. These microcoils perform remarkably well for extremely small samples [17] for reasons that are well understood [18]. The use of microcoils also reduces the size of the region of homogeneous magnetic field required for NMR, enabling the use of much smaller magnets [7]. We recently [19, 20] pioneered nanoliter-volume microcoil NMR in relatively low-field permanent magnets, paving the way toward a truly compact NMR system.

Halbach magnets [21] would commonly be considered well suited for compact NMR because they are extremely efficient; the magnetic material itself provides the flux return path, thus eliminating the heavy steel of a traditional magnet design. However, the rare-earth magnet materials generally show piece-to-piece variations of a few percent so these multipiece magnets must undergo major adjustments (shimming). The challenge of shimming any magnet rises with decreasing size; shimming efforts and designs [22, 23] rapidly drive the cost and complexity of the small magnet out of the realm of practical applications (B. Lown, Aster Enterprises, Acton, MA, USA, pers. commun.). We prefer the use of precision steel pole-caps and steel flux return paths in our small magnets since this simpler approach can meet the homogeneity, cost, and environmental insensitivity requirements of industrial applications; the extra weight of the steel is inconsequential for small enough magnets.

Here we present the first ^{1}H spectra acquired in such a magnet. In particular, the magnet weighs less than 700 g, has a volume of $(5\ \mathrm{cm})^3$, requires minimal adjustment, is impervious to strong external magnetic fields, and responds gracefully to temperature changes. Most importantly, a microcoil probe built for this magnet achieves 0.24 ppm resolution without the use of current shims on samples large enough to provide a signal-to-noise ratio (SNR) of 61 in a single data acquisition. While this cannot be considered high-resolution NMR, the resolution is sufficient to perform many useful spectroscopic tasks. When combined with single-board NMR spectrometer technology such as that from SpinCore (Gainesville, FL), our magnet and probe will be the first completely portable frequency-domain NMR spectrometer.

2 Materials and Methods

The magnet used for these experiments is a 0.96 T, 5 mm gap SmCo permanent magnet of dipole designed, built by Aster Enterprises [24]. The magnet housing is roughly a 5 cm cube, and its weight is 685 g. The proprietary design utilizes steel pole pieces and is enclosed by a steel flux return path. The specification for the magnet homogeneity is 1 ppm over a 0.5 mm diameter spherical volume. A photograph of the magnet is provided in Fig. 1.

Previously, one of the authors demonstrated the construction and performance of permanent-magnet-based microcoil NMR detectors built with sample tubes ranging from 170 to 550 μm outer diameter (o.d.) [20]. We showed that our resonant circuit, which utilizes an auxiliary inductor, performed well as a detector for nanoliter-scale samples, allowing the NMR signals to be detected without signal averaging. The probes achieved line widths of 0.12 ppm or better in a large 1 T permanent magnet. Hence, we know that our probe designs are capable of the resolution required for ^{1}H spectroscopy.

For our much smaller magnet, we hand wound [20] an 8-turn coil with 50 gauge enameled magnet wire of total diameter of 37 μm on a glass capillary with 400 μm o.d. and 300 μm inner diameter (i.d.) (in our nomenclature, this is a 400/300 capillary). The nominal sample volume of 21 nanoliters was chosen as a compromise between enclosing enough sample volume to provide adequate SNR per-

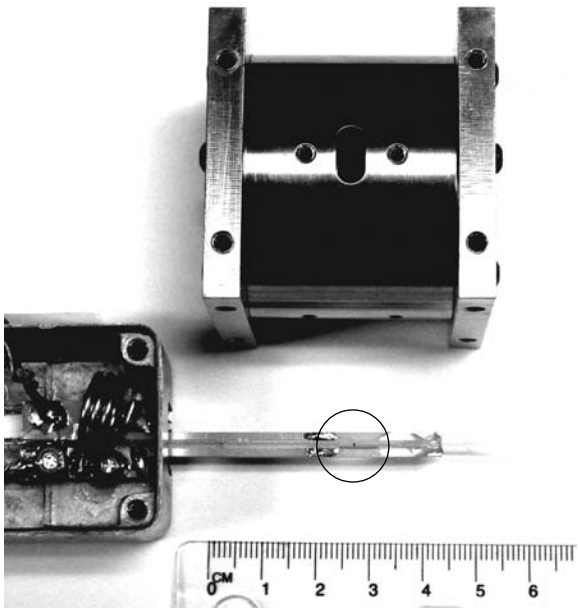

Fig. 1. Photograph of the magnet and microcoil probe. The microcoil is at the center of the circle. The aluminum box containing the tuning and matching circuit is open and visible on the left. The microcoil is supported by a long "tail" constructed from printed circuit board material, which also supports the fluid line.

formance and the need to probe the smallest practical region of the magnetic field in order to achieve a narrow line.

The 5 mm gap of the magnet imposes severe limitations on the form of the substrate supporting the microcoil. Therefore, we developed a simple printed circuit board (PCB) substrate that holds the microcoil near the end of an approximately 5 cm long tail, with about 1 mm wide traces of the 1 oz PCB (36 μm thick) copper providing the electrical connection between the microcoil and the remainder of the tuning and matching circuit. To deliver the fluid samples to the coil, a roughly 30 cm long section of 1/16 inch o.d., 400 μm i.d. fluorinated ethylene propylene tubing was glued to the 400/300 capillary with fast-setting two-component epoxy adhesive (5 minute epoxy). The PCB substrate was mounted in an aluminum probe housing with the tail protruding through one side. A photograph of the finished probe module is provided in Fig. 1.

To position the 400/300 probe in the magnet, the probe housing is mounted on an *XYZ* stage. The first time a new magnet is used, the probe is placed in the nominal center of the magnet at which point signal is readily detected by adjusting the operating frequency of the console. Fine adjustments of the probe position are then made while monitoring the free induction decay (FID). The effort to locate the optimal position ("sweet spot") of the probe for the first time may take a few hours; subsequent searches typically require a few minutes. The position of the sweet spot was observed to be stable from day to day so that only minor daily adjustments are required if the probe is left in the magnet. With only three adjustable parameters the shimming procedure is substantially easier than the traditional high-order case.

The NMR data in this work were all acquired with a compact magnetic resonance imaging console from MRTechnology [25]. We bypass the console's radio frequency (RF) power amplifier because less than a milliwatt of RF power is required to produce 120 μs $\pi/2$ pulses.

3 Results

Line Width and SNR. With the probe in the magnet as described above, we acquired the single-shot FID shown in Fig. 2a from 21 nanoliters of distilled water with dwell time of 1 ms and the detector band width of ± 500 Hz ($\Delta f = 1000$ Hz). The FID was time-shifted by 5 ms before Fourier transformation with no filtering or zero-filling (Fig. 2b). The line width is 9.9 ± 0.4 Hz at the full width at half-maximum, or 0.24 ppm, enabling nontrivial hydrogen spectroscopy as demonstrated by the ethanol spectrum in Fig. 2c. To our knowledge this is by at least an order of magnitude the highest resolution achieved in a handheld NMR magnet. The SNR of the FID (Fig. 2a) is 61, determined by taking the signal as the initial height of the FID and the noise as the standard deviation of the baseline points [20].

Field Mapping. We mapped the field of the magnet around the sweet spot with the *XYZ* stage. For each of the three orthogonal axes, the position of the sweet spot was determined and the probe was moved away from this location by 0.635 mm (0.025 inches). The spectrometer was set to acquire 4096-point FIDs every 0.4 s with a dwell time of 50 ms. Once data acquisition began, the probe

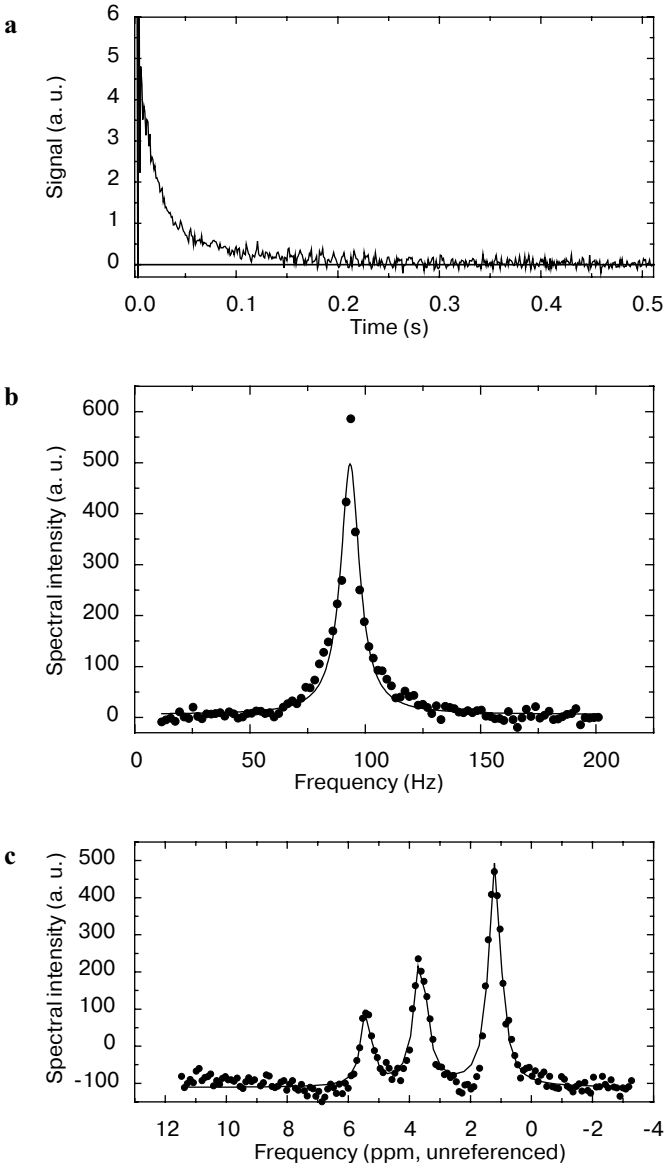

Fig. 2. Line width and SNR data. The sample volume is 21 nanoliters; the resonance frequency is 40.8 MHz. **a** Single-shot FID recorded from distilled water. The dwell time was 1 ms/point, and the filter setting was ± 500 Hz ($\Delta f = 1000$ Hz). The data were digitally shifted to be on resonance with the entire signal present in the single detector channel shown here. The SNR is 61 measured as the initial height of the FID (extrapolated back through the filter ringing) divided by the root-mean-square value of the baseline. **b** The Fourier transform of the FID in **a** calculated after the baseline correction and a time shift of 5 points (5 ms). The line is the Lorentzian fit, which, while not fitting the line shape in detail, provides a reasonable measure of the line width of 9.9 ± 0.4 Hz (0.24 ppm). **c** Single-shot spectrum of pure ethanol. The solid lines are a three-Lorentzian fit to the data as discussed in the text. The SNR of the highest peak is 45.

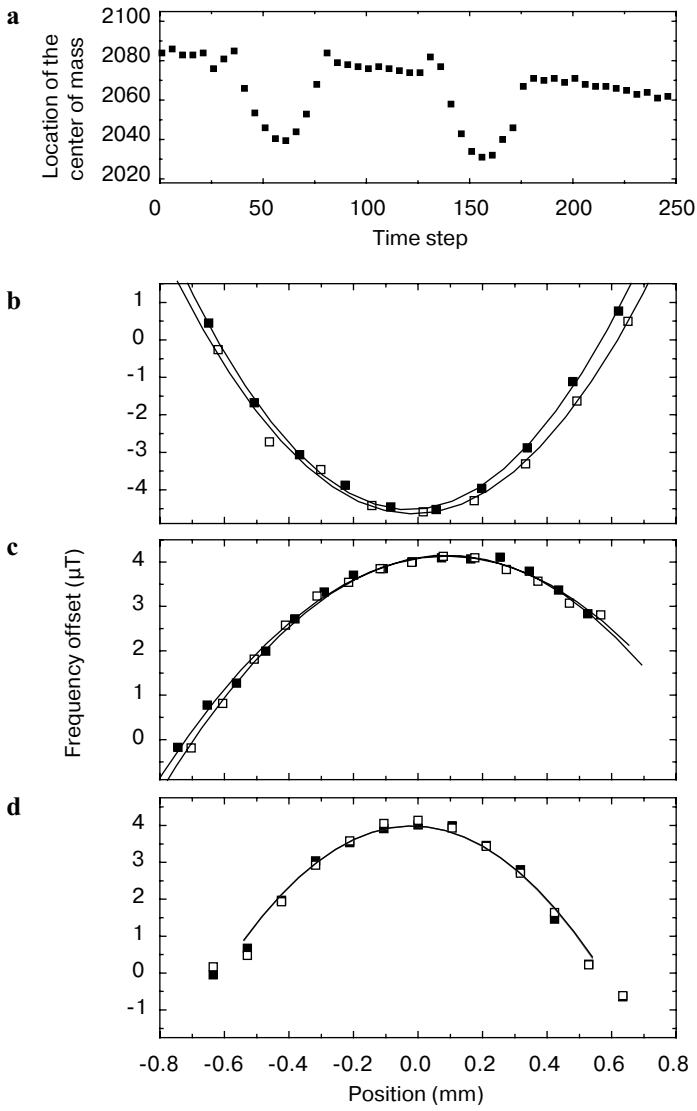

Fig. 3. Field map data. **a** The center of mass of the spectra acquired while moving across the magnet gap during the field mapping procedure described in the text. The overall drift of the field due to temperature changes is readily observed. **b**–**d** The relative field values along the three orthogonal axes. **b** The *Z*-axis is across the magnet gap; **c** the axial direction is along the access hole; **d** the transverse direction is orthogonal to both. The sweet spot is nominally at the point 0.0 on each axis.

was held stationary for several acquisitions and then manually moved at constant rate (about 40 μm/s) to a position 0.635 mm on the other side of the sweet spot. After parking the probe at this location for several more acquisitions, the probe was moved back to its original position at nominally the same rate. The acquisition of data along each axis required about 2 min.

The FIDs were Fourier transformed after shifting by 2 points to avoid filter ringing. The resulting spectra were visually examined and the center of mass of the peak was determined by eye for each time step. The reproducibility of this procedure was typically ±1 point (4.883 Hz); quick attempts to automate the procedure did not improve the precision due in part to the asymmetric line shapes acquired away from the sweet spot. The procedure yielded graphs like the one shown in Fig. 3a. The two traverses through the sweet spot of the magnet are clearly visible, as is the field drift with time caused by changing temperature. Using the known travel distance, the time axis of each traverse is converted to a position axis. The origin of the position axis is determined by identifying the time point at which the narrowest line is acquired. The uncertainties in converting the time axis to a position axis arise mostly from the determination of the timing of each end of the traverse; we estimate that the uncertainty in the length scale is ±10%. The zero of the position axis is more accurately known; its estimated uncertainty is ±2%.

After applying a linear correction to account for the field drift, the frequency axis yields the static local field offset. Combining this information with the position information derived as described above yields a plot of the field as a function of the position along each axis. The corresponding field plot for the data in Fig. 3a is given in Fig. 3b. The two traverses agree closely, especially in light of the rudimentary control and calculation of position. Field maps for the other two axes through the sweet spot are given in Fig. 3c and d. They also show good agreement between the two traverses. Note that the vertical scale, in μT, effectively serves as a ppm scale for this nearly 1 T magnet.

The field homogeneity in the vicinity of the sweet spot was characterized by quadratic fits to the field maps. Each traverse was fit separately as shown in Fig. 3. Only the central 0.9 mm of the transverse axis data was included in the quadratic fit.

4 Discussion

Line Width and Shape. The line width achieved in Fig. 2b represents a substantial improvement in resolution over previous results from handheld magnets. In Table 1, we provide a summary of the current state of the art as we know it. (We note that many of those systems employed homebuilt magnets while we rely on an established manufacturer.) Perlo et al. [22] has also achieved 0.25 ppm, but in a single-sided magnet configuration. We estimate, however, that their magnet is about 30 times heavier than ours. The same group [26] also achieved the next best resolution, using a similar magnet (without the exquisitely adjusted shims) but building an RF coil that closely matched their static field inhomogeneity. Their single-sided magnet will allow the study of fluids inside large objects but the relatively low field strength of the single-sided NMR magnet will limit its application, especially for spectroscopy, and it will be a challenge to migrate their carefully adjusted system into a magnetically inhomogeneous industrial setting.

Table 1. Portable NMR magnets.

Reference or source	Resolution (ppm)	Mass (kg)	Sample size (mm)	Field strength (T)
This work	0.25	0.6	0.3 o.d.×0.3	1
Perlo et al. [22]	0.25	20[a]	5×5×0.5	0.2
Perlo et al. [26]	8	15[a]	1 o.d.	0.2
Demas et al. [27]	17	2	0.32 o.d.×1	2
Moresi and Magin [7]	41	4[a]	3 o.d.×5	0.6
Manz et al. [28]	50	0.6	1.5 o.d.×1.8	1
Jachmann et al. [23]	56	5	0.25 o.d.×2	0.5
Marble et al. [31]	250	5	~5×10×10	0.1
Raich and Blümer [8]	700	11.4	18×18×30	0.3
Zhang et al. [32]	2250	17	1.2 o.d.×0.8	1
Hills et al. [33]	2300	2[a]	10×10×10	0.09

[a] Mass values have been estimated.

Demas et al. [27] has presented an effort similar to ours, using a light magnet possessing a higher field strength. However, their resolution is nearly 2 orders of magnitude coarser than our result, rendering it unsuitable for ^{1}H spectroscopy, which is also the case for the remaining entries in Table 1, including a recent portable NMR device by Manz et al. [28].

Earth's field devices [29, 30] which are capable of extraordinarily high resolution (albeit not for chemical shifts) are not included in Table 1. Prepolarization of the nuclear spins is used in these experiments in order to generate an adequate SNR, and it is this prepolarization apparatus that sets the weight scale, typically tens of kilograms. Furthermore, the resolution will be degraded even by very weak perturbations of the magnetic environment of the experiment. Our magnet is highly self-shielding; attaching a small NdFeB magnet (with measured magnetic field of 0.3 T at its surface) to the corner of our magnet caused only a 30% degradation of the line width and a 0.05% (500 ppm, 4.8 G) change in the center frequency, a trivial amount considering the strength of the perturbing magnet.

Our observed line width can be attributed to the static field distortions. The sample volume in the 400/300 probe has a diameter of 0.3 mm and a similar length. Hence the sample volume occupies nearly 1/4 of the position axes of the field plots in Fig. 3. We use the parabolic fits to calculate expected spreads of magnetic field values for our sample ranging from −0.32 to +0.39 ppm, which are 2–3 times worse than the observed line width. The most likely cause for this is a possible mismatch of the origins of the parabolas in the three directions, estimated to be about 25 μm. Shifting our field plots by this distance makes a substantial impact on the field spread calculation. Searching for the optimal location experimentally, on the other hand, finds the best compromise between the positive and negative deviations characterized in Fig. 3 and is not subject to limits on our knowledge of the coordinates of the sweet spot. Taking these and other issues into account, recalling the provenance of the field maps, and noting the sense of the disagreement, we find the factor of 2–3 discrepancy between the calculated field ranges and the measured line width to be acceptable. We further

note that the line shape in Fig. 2b is not Lorentzian. There is quite a lot of spectral power in the sides of the peak, which must come from the edges of the sample. The narrow part of the line comes from the sample region located in the flattest part of the field map.

SNR. Using the approach outlined previously [20], we can calculate the expected SNR of water in the 400/300 probe. Setting the geometrical factor $k_0 = 1$, we calculate SNR to be equal 155. Our measured value is 61, which we adjust upward to 73 to account for the preamplifier noise figure [20]. Hence our measured SNR is 47% of the expected value. Some decrease from 100% is expected since k_0 should have a value less than 1, but we expect k_0 to be roughly 0.6 on the basis of our previous work. The tuning inductor and PCB leads between the tuning elements and the microcoil contribute negligibly to the RF resistance of the resonant circuit. However, our probe's tail is unshielded, except where it lies inside the magnet. We attribute the excess noise in our measurements to environmental noise injected into the signal path via the unshielded portion of the probe's tail. We have seen that noise sources brought closer to the experiment makes the noise level worse by injecting unwanted coherent signals. Clearly, there is room for improvement through the implementation of simple RF shields but the 400/300 probe yields an adequate SNR for our present purposes without additional shielding.

Field Drift and Signal Averaging. Figure 3a shows a field drift of 2.1 Hz/s (51 ppb/s), typical in our SmCo magnet (temperature coefficient of about 300 ppm/K). Since our line is 10 Hz wide, we can signal average for only a few seconds without broadening the line appreciably. However, the field drifts without changing its shape as the temperature varies, which means that the long-term signal averaging can be implemented by frequency-shifting the individual acquisitions before summing. Of course, natural embellishments to this magnet would include improved thermal insulation, temperature control, and field frequency lock.

Ethanol Spectrum. The ethanol spectrum in Fig. 2c was fit with three Lorentzians. The relative areas of the curves $1.0:(2.1\pm0.2):(3.4\pm0.4)$ agree with the expected 1:2:3 ratio. The peak positions relative to the strongest peak are 3.65 ± 0.1 and 5.41 ± 0.02 ppm, while the expected positions are 3.65 and 5.275 ppm, an agreement that is even better than we expected.

The lines in the ethanol spectrum were twice as wide as those for the distilled water. The probe position required adjustment upon the replacement of water with ethanol and this adjustment is difficult to optimize on the multiline spectrum. It is likely that further efforts in position adjustment would improve the spectral resolution. Another effect we encountered while working with such small sample volumes is that the fluid in the system can move through the detector due to mechanical or thermal fluctuations elsewhere in the system. The sample volume accounts for less than 0.1% of the total system fluid volume, so even minor temperature changes can cause large displacements of the sample during the experiment, leading to the lifetime broadening. Ethanol's thermal expansion coefficient is six times that of water, making it more sensitive to this effect. Temperature control of the fluid handling system, along with reduction of the total system volume, should ameliorate this minor problem.

5 Conclusions

We demonstrated a subkilogram dipole permanent magnet and microcoil probe combination that achieves sufficient resolution to enable nontrivial ^{1}H spectroscopy in a hand-portable platform. This platform is light-weight, easy to use, and essentially independent of changes in its magnetic environment. The system achieves its performance without shim coils, specialized shimming techniques, careful matching of RF and static magnetic field, sophisticated pulse sequences, or field-frequency lock. The main challenge in using our device is in positioning the sample, which can be optimized in a few minutes and is stable from day to day. In conjunction with miniaturized NMR electronics, the magnet and the probe could form the first portable frequency-domain NMR spectrometer. Although our apparatus is limited to the study of fluids that can be injected into the probe, this is consistent with the vast majority of potential applications of compact NMR spectroscopy. Simple improvements, including shim coils, thermal isolation and stabilization, field-frequency locking, and better RF shielding, will improve performance and ease of use.

Acknowledgments

We thank Bob Lown of Aster Enterprises for useful discussions, and Shin Utsuzawa and Natalie Adolphi, both of New Mexico Resonance, for careful reading of the manuscript.

References

1. Gil, A.M., Belton, P.S., Hills, B.P.: Annu. Rep. NMR Spectrosc. **32**, 1–49 (1996)
2. Blümler, P., Blümich, B., Botto, R., Fukushima, E. (eds.): Spatially Resolved Magnetic Resonance. Wiley-VCH, New York (1998)
3. Ruan, R.R., Chen, P.L.: NMR Approach. Technomic, Basel (1998)
4. Coates, G.C., Xiao, L., Prammer, M.G.: NMR Logging Principles and Applications. Halliburton Energy Services, Houston (1999)
5. Stapf, S., Han, S.-I.: NMR Imaging in Chemical Engineering. Wiley-VCH, Darmstadt (2006)
6. Goloshevsky, A.G., Walton, J.H., Shutov, M.V., de Ropp, J.S., Collins, S.D., McCarthy, M.J.: Rev. Sci. Instrum. **76**, 024101 (2005)
7. Moresi, G., Magin, R.: Concepts Magn. Reson. B **19**, 35–43 (2003)
8. Raich, H., Blümler, P.: Concepts Magn. Reson. B **23**, 16–25 (2004)
9. Eidmann, G., Savelsberg, R., Blümler, P., Blümich, B.: J. Magn. Reson. A **122**, 104–109 (1996)
10. Kleinberg, R.L., Jackson, J.A.: Concepts Magn. Reson. **13**, 340–342 (2001)
11. Manz, B., Coy, A., Dykstra, R., Eccles, C.D., Hunter, M.W., Parkinson, B.J., Callaghan, P.T.: J. Magn. Reson. **183**, 25–31 (2006)
12. Hills, B.P., Wright, K.M.: J. Magn. Reson. **178**, 193–205 (2006)
13. Goodson, B.: Phys. World **19**, 28–33 (2006)
14. www.cryogenic.co.uk
15. www.foxboronmr.com
16. Peck, T.L., Magin, R.L., Lauterbur, P.C.: J. Magn. Reson. B **108**, 114–124 (1995)
17. Seeber, D.A., Cooper, R.L., Ciobanu, L., Pennington, C.H.: Rev. Sci. Instrum. **72**, 2171–2179 (2001)
18. Webb, A.G.: Prog. Nucl. Magn. Reson. Spectrosc. **31**, 1–42 (1997)

19. Sillerud, L.O., McDowell, A.F., Adolphi, N.L., Serda, R.E., Adams, D.P., Vasile, M.J., Alam, T.M.: J. Magn. Reson. **181**, 181–190 (2006)
20. McDowell, A.F., Adolphi, N.L.: J. Magn. Reson. **188**, 74–82 (2007)
21. Halbach, K.: Nucl. Instrum. Methods **169**, 1–10 (1980)
22. Perlo, J., Casanova, F., Blümich, B.: Science **315**, 1110–1112 (2007)
23. Jachmann, R.C., Trease, D.R., Bouchard, L.S., Sakellariou, D., Martin, R.W., Schlueter, R.D., Budinger, T.F., Pines, A.: Rev. Sci. Instrum. **78**, 035115 (2007)
24. www.asterenterprises.com
25. www.mrtechnology.co.jp/eng/index2.html
26. Perlo, J., Demas, V., Casanova, F., Meriles, C.A., Reimer, J.R., Pines, A., Blümich, B.: Science **308**, 1279–1280 (2005)
27. Demas, V., Herberg, J., Malba, V., Bernhardt, A., Evans, L., Harvey, C., Chinn, S.C., Maxwell, R.S., Reimer, J.: J. Magn. Reson. **189**, 121–129 (2007)
28. Manz, B., Benecke, M., Volke, F.: J. Magn. Reson. **192**, 131–138 (2008)
29. Callaghan, P.T., Eccles, C.D., Seymour, J.D.: Rev. Sci. Instrum. **68**, 4263–4270 (1997)
30. Appelt, S., Kühn, H., Häsing, F.W., Blümich, B.: Nat. Phys. **2**, 105–109 (2006)
31. Marble, A.E., Mastikhin, I.V., Colpitts, B.G., Balcom, B.J.: J. Magn. Reson. **186**, 100–104 (2007)
32. Zhang, X., Mahesh, V., Ng, D., Hubbard, R., Ailiana, A., O'Hare, B., Benesi, A., Webb, A., in: Hiller, J.-A. (ed.) Proceedings of the COMSOL Multiphysics Conference, Held at Boston, Mass., October 23–25, 2005. COMSOL, Burlington, Mass. (2005)
33. Hills, B.P., Wright, K.M., Gilles, D.G.: J. Magn. Reson. **175**, 336–339 (2005)

Authors' address: Andrew F. McDowell, ABQMR Inc., 2301 Yale Boulevard SE, suite C-2, Albuquerque, New Mexico 87106, USA
E-mail: mcdowell@abqmr.com